RSC Advances

ROYAL SOCIETY OF CHEMISTRY

www.rsc.org/advances

A novel kind of nanoflakes zirconia-carbon (ZrO_2-C) composites which exhibited much higher adsorption capacity to TCP

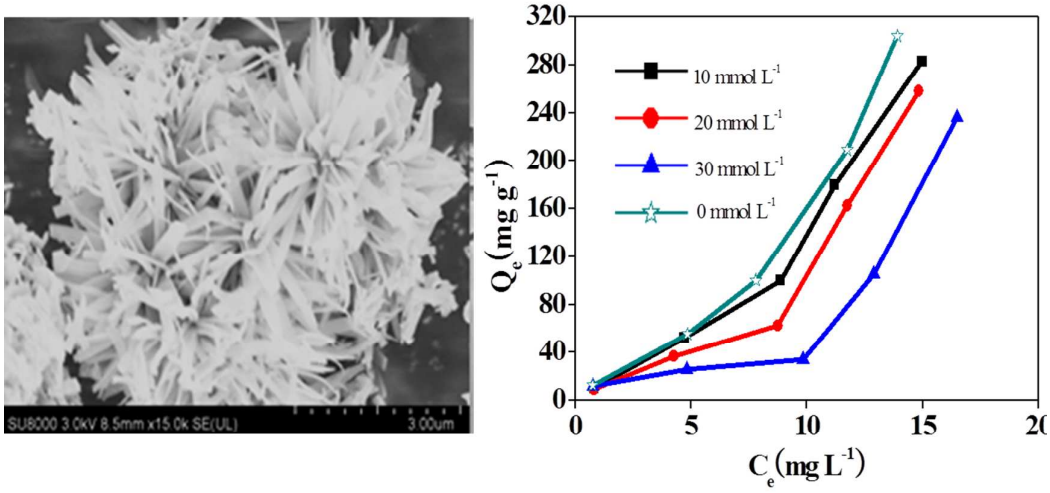

Synthesis of flower-like ZrO_2-C composites for adsorptive removal of trichlorophenol from aqueous solution

Yixin Tan [a,b,c], Lehui Zhu [a], Hongyun Niu[b,*], Yaqi Cai[b], Fengchang Wu[c], Xiaoli Zhao[c,*,]

[a]*Department of Resources Environmental and Chemical Engineering of Nanchang University, Jiangxi, Nanchang Province, 330031, China*

[b]*State Key Laboratory of Environmental Chemistry and Ecotoxicology of Research Center for Eco-Environmental Sciences, Chinese Academy of Sciences, Beijing 100085, China*

[c]*State Key Laboratory of Environmental Criteria and Risk Assessment, Chinese Research Academy of Environmental Sciences, Beijing, 100012, China*

***Corresponding author: Hongyun Niu**

Chinese Academy of Sciences

Research Center for Eco-Environmental Sciences

P. O. Box 2871

Beijing 100085, China

E-mail Address: hyniu@rcees.ac.cn

Tel: (086) 010-62849182;

Fax: (086) 010-62849182

ABSTRACT

In the current study, a novel kind of nanoflakes zirconia-carbon (ZrO_2-C) composites were synthetized through a simple method by using gallic acid and $ZrCl_4$ as precursor. The as-synthesized ZrO_2-C composites possessed high specific surface areas and chrysanthemum-like structure. High-resolution transmission electron microscope, X-ray photoelectron spectroscopy, infrared spectroscopy, X-ray diffraction, and Raman analysis revealed that ZrO_2-C composites were composed of graphitized carbon and numerous ZrO_2 nanoparticles (3-4 nm in diameter). ZrO_2-C composites were successfully used as adsorption materials to remove 2, 4, 6-trichlorophenol (TCP) from simulated water samples. The results showed that ZrO_2-C exhibited much higher adsorption capacity to TCP than some reported carbon materials. The hydrophobic interaction and/or π–π stacking interaction between TCP and carbon phase, hydrogen bonding with functional groups of ZrO_2-C, and metal-anion binding with ZrO_2 nanoparticles contributed to the high adsorption ability. Generally, TCP uptake was favorable at acidic environment and increased with the initial TCP concentration and temperature, the adsorption process obeyed the pseudo-second-order kinetics model and the adsorption isotherms could be better described by the Freundlich equation.

Key Words: Gallic acid, zirconia-carbon composites, Chrysanthemum-like structure, Adsorption, Trichlorophenol

Introduction

Chlorophenols are widespread used in petroleum refining, plastic, rubbers, pharmaceuticals, disinfectants, wood preserving, steel industries the pulp and paper industry. Due to their carcinogenic and mutagenic nature and high resistance to

biodegradation, chlorophenols pollutants are now receiving great concern[1, 2]. Many efforts have been made for the physicochemical (such as adsorption[1-14], ozonation[15-17], and electrochemical oxidation[18]) and biological treatment of chlorophenol-rich wastewater[19, 20].

Over the last century, much research has occurred in the area of removal of chlorophenols by carbon materials, including activated carbon, carbon nanotubes, graphene, and mesoporous carbon, which demonstrates high removal efficiency to organic pollutants[1-10]. Soil, metal oxides and zeolite have been explored as adsorbents to remove chlorophenols from aqueous solutions as well[11-14, 21-23]. The sorption of chlorophenols on these inorganic adsorbents proceeded via different reaction mechanisms, including inner- or outer-sphere coordination, H-bonding, ligand exchange between the OH groups of phenolic compounds and the active sites (hydroxyl groups) of adsorbents, and complexation of phenolate anions with metal ions on the surface of adsorbents. Yousef et al. showed that the adsorption capacity of chlorophenols onto natural zeolites reached 0.32 mmol g^{-1}, which was comparable with those obtained by some carbon materials[11]. Therefore, metal oxides, soil or zeolites can be regarded as potential adsorbents to remove chlorophenols from environmental waters.

Herein a kind of combination of carbon materials and metal oxides has been put forward, which can provide multiple adsorptive sites and different interaction mechanisms to chlorophenols. Gallic acid (GA), a phenolic compound belonging to the hydroxybenzoic acids, is highly present in legums (onions, black radish, hops), fruits (grapes, some red fruits), nuts (gallnuts) and beverages (team wine, beer). GA can form a complex with Fe(II), Fe(III), Cu(II), Al(III), Zr(IV), and Mo(VI), et al[24-28]. GA has been used in the green synthesis of AgNPs and AuNPs as well[29]. However, to the best of our knowledge, GA has not been utilized as organic ligands

to synthesize hierarchical structured nanoparticles. In the current study, we use GA as both organic ligands and carbon precursor to prepare carbon and metal oxides composites. Zirconium oxides are used as metal precursors due to the excellent chemical stability of Zr-based inorganic or organic materials[30]. The synthesis method of ZrO_2-C composites is very simple with high yields. The as-prepared ZrO_2-C composites possess chrysanthemum-like structure and are used as adsorbents to remove 2, 4, 6-trichlorophenol from water.

2. Experimental section

2.1. Chemicals and materials

Zirconium tetrachloride, hydrochloricacid (HCl, 36%~38%), ethanol, and N,N-dimethylformamide (DMF, 99.5%) were purchased from Sinopharm Chemistry Reagent Co., Ltd. (Beijing, China). 2, 4, 6-trichlorophenol (TCP) and gallic acid were obtained from J&K Chemical Ltd. (Beijing, China). TCP (100 mg L^{-1}) was prepared and diluted to certain concentration when it was necessary. Ultrapure water used in all of the experiments was prepared by using Milli-Q SP reagent water system (Millipore, Bedford, MA, USA).

2.2 Synthesis and structure of ZrO_2-C

Firstly, $ZrCl_4$ (0.933g) was dissolved in 5 mL of ethanol, and then mixed with 65 mL of DMF; after that 0.753g of gallic acid were added to the mixture under stirring. The reaction solution was transferred in Teflon-lined stainless-steel autoclave, sealed to heat at 403 K for 24 h. The white products were washed with DMF three times and soaked in ethanol for three days (change ethanol each day) and dried at 323 K under vacuum environment for 12h. Finally, the product (1.348g) was removed to a quartz tube to carbonize under the protection of nitrogen at 1073 K for 4h.

97 **2.3 Characterization of the material**

98 The size and morphology of the synthesized materials were surveyed using a
99 Hitachi S-5500 field-emission scanning electron microscope (FE-SEM, Tokyo, Japan)
100 equipped with an energy dispersive X-ray spectrometer (SEMEDX, Tokyo, Japan), a
101 JEOL JEM-2010 high-resolution transmission electron microscope (HRTEM, Kyoto,
102 Japan), and a Hitachi H-7500 transmission electron microscope (TEM, Tokyo,
103 Japan). The crystalline phase of products were analyzed using X-ray powder
104 diffraction (XRD, Almelo, Netherlands) by using a Cu Ka radiation ranging from 5°
105 to 90° with a resolution of 0.02°. BET methods were adopted to measure the surface
106 area, pore size and volume (ASAP2000 V3.01A; Micromeritics, Norcross, GA).
107 FTIR spectra were recorded in the range of 4000-400 cm^{-1} by a NEXUS 670 Infrared
108 Fourier Transform Spectrometer (Nicolet Thermo, Waltham, MA) after pelletizing
109 with KBr. Thermogravimetry and differential thermal analysis (TG-DTA) for freeze-
110 dried samples were carried out on a Mettler Toledo Star TGA/SDTA 851 apparatus,
111 and the temperature ranged from room temperature to 1173 K with rising rate of 10
112 K min-1. The sample chamber was purged with dry nitrogen. To detect the
113 composition and chemical state of elements on the surface of materials, the products
114 were analyzed using X-Ray photoelectron spectroscopy (XPS) collected on an
115 ESCA-Lab-200i-XL spectrometer (Thermo Scientific, Waltham, MA) with
116 monochromatic Al Ka radiation (1486.6 eV).

117 **2.4 Absorptive removal of pollutants**

118 Absorption experiments were conducted in the simulated polluted water (10mL) in
119 batch experiment. The concentration of adsorbent was 0.02g L^{-1}. The solution pH
120 was adjusted with HCl and NaOH to desired values, and the ionic strength was
121 adjusted with 1 M NaCl. The effect of initial pH on the sorption of TCP was studied

in the pH range of 3.0-10.0. Dynamic experiments were operated under the condition of temperature 303K and TCP 20 mg L^{-1}. The influence of ionic strength was tested by adding NaCl (10, 20, and 30 mM) in solution. To investigate the thermodynamic properties, adsorption isotherms were recorded in 10 mL of TCP solution with concentrations of TCP varying from 0.5 to 20 mg L^{-1} at 303K, 313K, and 323K, respectively. All experiments were conducted in triplicate, and average results were reported.

We calculated the maximum and equilibrium adsorption quantity by measuring the concentration of the original TCP and equilibrium TCP in the whole process. The formula of adsorption as follows：

$$q_e = \frac{(C_0 - C_e)\ V}{m} \quad (1)$$

where q_e (mg g^{-1}) is on behalf of the equilibrium adsorption quantity; C_0 (mg L^{-1}) and C_e (mg L^{-1}) is the original and equilibrium concentration of TCP; m (g) is the the quality of adsorbent; and V (L) is the volume of the solution which is original.

The dosage of TCP was detected by HPLC system equipped with a DIONEX HPLC pump (P680), a thermostatted column compartment (TCC-100) and a photodiode array detector (PDA-100). Separations were conducted on a Dikma C18 column (250 ×4.6 mm; 5 μm). The mobile phase for TCP was acetonitrile: 2% HAc (80:20 V/V) at a flow rate of 1 mL min^{-1}. The wavelength was set at 290 nm.

3. Results and discussion

3.1 Characterization and properties of adsorbents

Fig 1 shows the TEM and SEM images of the as-prepared materials. The Zr-GA particles shape like chrysanthemum with the size of about 4μm (Fig. 1A and 1B). High resolution TEM image of Zr-GA indicates that this material is composed of

nanoflakes (Fig. 1C) with ~350 nm in width. After carbonization, the chrysanthemum-like shape remains, the particle size of ZrO_2-C composites decreases to about 2μm (Fig.1D and E). Fig. 1F and 1G demonstrate that the nanoflakes of Zr-GA have reduced to about 100-300 nm in width and contain numerous tiny nanoparticles (3-4 nm in diameter) which should be ZrO_2.

The crystal phases of the samples are investigated by XRD analysis. **Fig. 2** displays that the XRD pattern of Zr-GA is totally different with that of ZrO_2 and GA powder. The peaks occurring at 7.2°, 9.0°, 11.3°, 16.8°, 17.3°, 21.3°, 23.5°, 26.3°, 28.5°, 31.1°, 36.6° were basically conformed to Zr-MOF which are synthesized by zirconium metal salts and organic compounds with carboxyl group in other studies[31-34]. Since the organic ligands (gallic acid) in our study are different with the traditional organic ligands used to synthesize MOF, a little deviation of the some peaks may occur. The characteristic peaks suggest the chelation of Zr atoms with GA in Zr-GA. In the XRD pattern of ZrO_2-C, the distinguishing characteristic peaks appear at $2\boldsymbol{\theta}$=30.1°, 35.4°, 50.2°, and 60.2°, which can be attributed to the (101), (002), (112), and (211) diffraction planes of the tetragonal zirconia[35, 36].

Fig. 3A shows the IR spectra of GA, Zr-GA and ZrO_2-C. In the spectrum of GA, the broad peaks at 3368 cm^{-1} and 3287 cm^{-1} are corresponding to the phenolic groups. The peaks ranged in 3200-2500 cm^{-1} are associated with the bending or stretching vibration of carboxylic acid O-H and C-H in aromatic groups. The sharp peak at 1701 cm^{-1} is due to the C=O stretching vibration from carboxylic groups. The peaks in the region of 1500-1000 cm^{-1} are assigned to the stretching vibration of C-O, binding adsorption of O-H of carboxylic and phenolic groups and C-H of aromatic rings (Fig 3B). After interaction with Zr (IV), the O-H stretching band in the region of 3400-2500 cm^{-1}, Zr-O-H bending peaks at 1332 cm^{-1}, and O-H of carboxylic groups bending band at 1029 cm^{-1} disappear, indicating that all the phenolic groups

and carboxylic groups in GA chelate with Zr. Correspondingly, C=O stretching bend in the spectrum of Zr-GA shift to low frequency, and two characteristic bands of the carboxylate groups (COO-) between 1300 and 1600 cm^{-1} appear. Asymmetrical stretching of carboxylate groups occurs at 1500 cm^{-1} with stretching at 1426 cm[37]. These results indicate that all the carboxylic and phenolic groups in the molecules interact with Zr. Actually, the carboxylic groups are vital for the formation of chrysanthemum-like structure of materials. If tannic acid is adopted as linker, the hierarchical morphology of the as-prepared products could not be observed. In the spectrum of ZrO_2-C, the characteristic peaks for carboxylic groups, phenolic groups and benzene rings generally disappear, suggesting the successful carbonization of GA; the broad peaks in the region of 3600-3300 cm^{-1}, and 1670-1550 cm^{-1} are corresponding to the surface-sorbed water and hydroxyl groups of carbon materials.

XPS was adopted to investigate the elemental composition on the surface of Zr-GA before and after carbonization. Curve-fitting of the O1s and Zr3d lines for both materials employed Gaussian (20%)-Lorentzian (80%) peak-shapes, respectively (defined in Casa XPS as GL (80)). The O1s core levels for Zr-GA present three main components related to C-OH, COO- and H_2O species. (Fig. 4A). The Zr3d spectra of Zr-GA are characterized by doublet terms of Zr3d3/2 and Zr3d5/2 due to spin-orbit coupling, and the positions of Zr3d5/2 and Zr3d3/2peaks locate at 182.5 and 185.0 eV (Fig. 4B), respectively, which is consistent with the zirconium (IV) cations coordinated carboxylic oxygens of organic ligands in zirconium metal-organic framework and amine-functionalized zirconium metal-organic framework[38]. After carbonization, the O1s core-level shifts to lower binding energies with the disappearance of H_2O species and significant decrease of the contents of C-OH and COO- species, meanwhile, the Zr-O bond appears. The Zr3d spectra intensity of ZrO_2-C increases obviously, and the positions of Zr3d peaks are observed to shift to

lower binding energies (182.4 and 184.8 eV, respectively). Generally, the Zr 3d spectra of Zr-GA and ZrO_2-C are in good agreement with the reported values for Zr(IV) cations. Wang[39] and co-workers found that the binding energy of the Zr3d in hybrid ZrO_2/polymer nanoparticles was higher than that in ZrO_2, suggesting the formation of chemical bonds between the Zr(IV) and the organic components. Similar with the case of zirconium metal-organic framework, we deduce that the Zr atoms coordinate the oxygen atoms from gallic acids in the chrysanthemum-like Zr-GA structure; while zirconium transforms to ZrO_2 in the process of carbonization. In Raman spectrum of ZrO_2-C (**Fig. 4C**), two peaks centered at 1580 (G-line) and 1350 cm^{-1} (D-line), attributing to in-plane vibrations of crystalline graphite and disordered amorphous carbon, respectively, suggesting that the GA linkers are successfully graphitized. The above-mentioned results imply that ZrO_2-C is composed of ZrO_2 and graphitized carbon.

The TGA curve of ZrO_2 (**Fig. 4D**) shows slight weight decreases below 473 K due to the initial loss of water. When the heat temperature is above 623 K, carbon phase in the ZrO_2-C decomposes promptly suggesting the oxidation of carbon. The percent remaining after 713 K can be regarded as absolutely ZrO_2. According to the TGA result of ZrO_2-C, the mass percentage of carbon is estimated to be 40 %. The N_2 adsorption/desorption isotherm and calculated pore size distribution of ZrO_2-C (**Fig. 4E**) suggests that the adsorption process conform to the IV-type with a H3-type hysteresis loops, indicating that the pore belongs to mesoporous. The total pore volume of ZrO_2-C was determined to be 0.25 cm^3 g^{-1}. The average pore size calculated from desorption branch of the N_2 isotherm by Barrett-Joyner-Halenda (BJH) method was 3.8 nm, and the Brunauer-Emmett-Teller (BET) surface area of the obtained ZrO_2-C composite was 79.4 m^2 g^{-1}.

3.2 Adsorption kinetics

The kinetics of TCP adsorption onto ZrO_2-C was analyzed using both the pseudo-first-order and pseudo-second order kinetic models. The pseudo-first-order kinetic model is defined as follows:

$$\ln(q_e - q_t) = \ln q_e - k_1 t \quad (2)$$

where q_e (mg g^{-1}) and q_t (mg g^{-1}) are the amounts of TCP adsorbed at equilibrium and any time t (h), respectively, and k_1 (h^{-1}) is the adsorption rate constant.

The pseudo-second-order constants were calculated according to equation (3):

$$\frac{t}{q_t} = \frac{1}{K_2 q_e^2} + \frac{1}{q_t} t \quad (3)$$

where k_2 (g $mg^{-1} \cdot h^{-1}$) is the pseudo-second-order rate constant.

As shown in **Fig. 5A**, TCP adsorption increased rapidly with time and reached a constant value in 10 h. The kinetic parameters and correlation coefficient (R^2) obtained for the plots are given in **Table 1**. As a result, the R^2 value of pseudo-second-order kinetic model is 0.994 and the calculated $q_{e,cal}$ is very close to the experimental $q_{e,exp}$, demonstrating that the kinetics data fits well with the pseudo-second-order kinetic model.

3.3 Effect of pH

The pH of solution is one of the main factors affecting the adsorption capacity of compounds that can be ionized. The surface chemistry of carbon adsorbents may change with solution pHs. These effects may result in significant alterations in the removal efficiency of TCP depending on the pHs. **Fig. 5B** shows that the uptake of TCP on ZrO_2-C is superior in acid solution to those in neutral and alkali solutions, which is resemble with the optimum pH range observed on other carbonaceous materials[37, 40, 41]. In the current study, the adsorption capacity of TCP on ZrO_2-C is the highest at pH 4.0, and then declines with rising of solution pH. Since the pK_a of TCP is pH 5.99[42], the majority of TCP exists in the neutral and unionized forms in

acid solution; and ionizes gradually and becomes negatively charged as solution pH is higher than 5.99. To interpret the effect of solution pH on TCP adsorption, we also measured ζ-potentials of ZrO_2-C in aqueous solutions. The isoelectric point (IEP) of ZrO_2-C is found at about pH 3.5 (**Fig. 5C**). At pH 3.5-4.0, both TCP and ZrO_2-C surface are neutral, which favors the hydrophobic interaction and/or π–π stacking interaction between TCP and ZrO_2-C. When the solution pH is lower than 3.5, the surface of the material is positively charged and the hydrophobic interaction between TCP and ZrO_2-C is weakened. So the adsorption capacity will decline under the condition of strong acid (pH<3.5). On the other hand, the neutral formed TCP also can form H-bonds with the oxygen-containing groups of carbon phase and ZrO_2 nanoparticles of the adsorbents.

In neutral and alkaline solution, electrostatic repulsions between the negative surface of ZrO_2-C and anionic TCP are expected, leading to decreased adsorption of TCP on ZrO_2-C. However, the downshift of TCP sorption in the pH range 6-10 is fairly slow, and the sorption capacity is still considerable at pH 12. This trend is obviously different with that obtained on most carbon materials such as graphene and graphene oxide[6], multi-walled carbon nanotubes[7], and surfactant-modified bentonite[6]. It was reported that the phenolate anions can complex with metal ions on the metal oxides, and zeolite surface, which proceeds via a kind of charge transfer from phenolate anions to empty d-orbitals of metal (such as Si, Al, Fe, Ti, Mn) on the surface of metal oxides[11-13, 21-23]. Okolo et al. suggested that the benzene ring (π electron) rather than the hydroxyl substituent of phenols interacts with synthetic zeolite surface[23]. Karunakaran and co-workers[43] assumed that the acidic sites on the surface of ZrO_2 may coordinate to the phenolic oxygen and/or the basic O^- group may be involved in hydrogen bonding with the –OH group of phenol. Since the electron density of phenol rings increases with solution pH, we believe that the

considerate adsorption of TCP on ZrO_2-C composites at higher solution pH result from complexation of TCP anions with Zr ions on the surface of large number of inlaid ZrO_2 NPs. On the other hand, in our previous work, we used magnetic mesoporous carbon which is composed of graphitic carbon and Fe_3C/α-Fe, as adsorbents to remove TCP as well. The specific surface area and carbon content of this material (220 m^2g^{-1} and 54.5%, respectively) are larger than those of ZrO_2-C synthesized in this study. However, the adsorption capacity of the magnetic mesoporous carbon to TCP at 303 K was much lower than that achieved on ZrO_2-C at pH 4. We deduce that the adsorption of TCP onto ZrO_2-C proceeds via hydrophobic interaction and/or π–π stacking interaction with carbon phase, hydrogen bonding with functional groups of ZrO_2-C, and/or complexation with Zr(IV) cations (especially at high solution pH).

3.4 Adsorption isotherm

The effect of solution temperature on TCP adsorption was investigated by varying the temperature at 303, 313 and 323 K, respectively. As a result, the adsorption capacity of TCP on ZrO_2-C enhances slightly with temperature, indicating the endothermic nature of the sorption process. Langmuir and Freundlich isotherm models were used to study the relationship between the adsorption quantity of TCP onto ZrO_2-C and its equilibrium concentration in water solution. The Langmuir model is widely used for the adsorption assuming that takes place specific homogeneous; while the Freundlich model assumes that the binding takes place on a heterogeneous adsorption surface with multilayer adsorption.

The linear form of the Langmuir isotherm equation is expressed as:

$$\frac{C_e}{q_e} = \frac{1}{K_L Q_0} + \frac{1}{Q_0} C_e \quad (4)$$

where Ce (mg L^{-1}), q_e (mg g^{-1}) and Q_0 (mg g^{-1}) are equilibrium concentration,

equilibrium adsorption quantity and single largest adsorption quantity, respectively. K_L is a constant related to the free energy of the adsorption (L mg^{-1}).

The logarithmic form of the Freundlich equation is described as following:

$$\ln q_e = \ln K + \frac{1}{n} \ln C_e \quad (5)$$

where K_F ((mg g^{-1})(L mg^{-1})1/n) and n are the Freundlich constants that point to the sorption capacity and adsorption intensity of the adsorbent, respectively.

Table 2 lists the constants and correlation coefficients gained from the two isotherm models. The Freundlich model yields better fit with higher R^2 values (higher than 0.986), indicating that the Freundlich isotherm is more suitable in describing the adsorption of TCP on ZrO_2-C. The 1/n value obtained from the Freundlich model is below 1 representing that adsorption of TCP on the ZrO_2-C is favorable. This result is consistent with TCP sorption on other carbon materials such as Loosestrife-based activated carbon[8], activated clay[12] and commercial grade coconut shell-based activated carbon[4].

Because TCP sorption on ZrO_2-C does not fit well to Langmuir equation, we can make a coarse estimate of the adsorptive ability of ZrO_2-C to organic pollutants by comparing the adsorption capacity calculated at a certain concentration with those obtained by other adsorbents reported in literature. The results are listed in Table 3. In despite of its relatively low specific surface areas and small porous volume, the sorption ability of ZrO_2-C to TCP is much higher than those obtained on many kinds of carbon-based materials reported previously. This may result from the joint contribution of ZrO_2 NPs and carbon phase of ZrO_2-C adsorbents to TCP sorption.

3.5 Adsorption thermodynamics

The thermodynamic equation is as following:

$$\ln K_d = \frac{\Delta S^0}{R} - \frac{\Delta H^0}{RT} \quad (6)$$

$$\Delta G^0 = \Delta H^0 - T\Delta S^0 \quad (7)$$

In the formula 6 K_d is the distribution coefficient of adsorbent, equal to q_e/c_e, R (8.314 J mol^{-1} K^{-1}) is the universal gas constant, T (K) is the temperature. ΔG^0 can figure up by ΔH^0 and ΔS^0.

The values of the thermodynamic parameters for the adsorption of TCP on mesoporous carbon materials are listed in Table 4. The value of ΔH° is positive suggesting that the reaction is endothermic, which is consistent with the result that TCP uptake increases with temperature. If ΔH° is higher than 40 kJ mol^{-1}, the adsorption process is supposed to proceed via chemisorption; while for values less than 40 kJ mol^{-1}, the adsorption process is of physical nature. The value of ΔH° is 8.7 kJ mol^{-1}, indicating that the main interaction between TCP and mesoporous carbon materials is of physical nature. The positive value of ΔS° suggests that the adsorption is irreversible. The negative value of ΔG° shows the spontaneous nature of the adsorption process.

3.6 Effect of ionic strength

The effect of ionic strength on TCP adsorption was investigated by conducting adsorption equilibrium experiments with different concentrations of NaCl at pH 4. As shown in **Fig. 5D**, the adsorption capacity of ZrO_2-C to TCP decreases by 7, 15 and 23% as the NaCl concentration is 10, 20, and 30 mM, respectively. This result indicates that the hydrophobic interaction and/or π-π stacking interaction between TCP and ZrO_2-C are stronger than non-specific electrostatic interactions, since the electrostatic interactions can be weakened by increased ionic strength of the solution.

4. Conclusion

We have synthesized ZrO_2-C composites with chrysanthemum-like morphology using a simple method with high yield. The ZrO_2-C composites exhibit excellent water stability and remarkable adsorption capacity to chlorophenols. The hydrophobic interaction and/or π-π stacking interaction and hydrogen-bonds between TCP and ZrO_2-C contribute to the fantastic adsorption of TCP on the material. Besides, ZrO_2 nanoparticles embedded in the carbon phase can form metal-anion bonds with TCP, which is responsible for the reasonable adsorption ability of ZrO_2-C to TCP even in weak alkali solution. The adsorption of TCP on ZrO_2-C is slightly influenced by temperature and ionic strength. These results provide effective method and reference for the removal of TCP in wastewater.

Ackowledgments

This work was jointly supported by National Basic Research Program of China (2015CB93203); Strategic Priority Research Program of the Chinese Academy of Sciences (XDB14010201), State Environmental Protection Welfare Scientific Research Project (201409037), and the National Natural Science Foundation of China (21277152, 21277002, 41222026).

Reference

1. R. S. Ojha Priyanka, Singh Kunwar, *S. Afr. J. Chem. Eng.*, 2014, **19**, 1-21.
2. D. Krishnaiah, S. M. Anisuzzaman, A. Bono and R. Sarbatly, *J. King Saud Univ. Sci.*, 2013, **25**, 251-255.
3. S. Wang, H. Niu, T. Zeng, X. Ma, Y. Cai and X. Zhao, *Cryst. Eng.Comm.*, 2014, **16**, 5598.
4. M. Radhika and K. Palanivelu, *J. Hazard. Mater.*, 2006, **138**, 116-124.
5. B. H. Hameed, I. A. W. Tan and A. L. Ahmad, *Chem. Eng. J.*, 2008, **144**, 235-244.
6. Z. Pei, L. Li, L. Sun, S. Zhang, X.-q. Shan, S. Yang and B. Wen, *Carbon*, 2013, **51**, 156-163.
7. G. C. Chen, X. Q. Shan, Y. S. Wang, B. Wen, Z. G. Pei, Y. N. Xie, T. Liu and J. J. Pignatello, *Water Res.*, 2009, **43**, 2409-2418.
8. J. Fan, J. Zhang, C. Zhang, L. Ren and Q. Shi, *Desalination*, 2011, **267**, 139-146.

9. C. Namasivayam and D. Kavitha, *J. Environ. Eng. Sci.*, 2004, **46**, 217-232.
10. S. Liu, S. Li, H. Niu, T. Zeng, Y. Cai, C. Shi, B. Zhou, F. Wu and X. Zhao, *Microporous Mesoporous Mater.*, 2014, **200**, 151-158.
11. R. I. Yousef and B. El-Eswed, *Colloids Surf. A*, 2009, **334**, 92-99.
12. B. H. Hameed, *Colloids Surf. A*, 2007, **307**, 45-52.
13. Y. Zhang, R. G. Mancke, M. Sabelfeld and S. U. Geissen, *J. Hazard. Mater.*, 2014, **271**, 178-184.
14. T. S. Anirudhan and M. Ramachandran, *J. Water Process Eng.*, 2014, **1**, 46-53.
15. J. A. Mielczarski. J. Bandara, J. Kiwi, *Appl. Catal. B Environ.*, 2001, **34**, 321-333.
16. H. Peng, J. Cui, H. Zhan and X. Zhang, *Chem. Eng. J.*, 2015, **264**, 316-321.
17. M. Pera-Titus, V. García-Molina, M. A. Baños, J. Giménez and S. Esplugas, *Appl. Catal. B*, 2004, **47**, 219-256.
18. H. Wang and J. L. Wang, *J. Hazard. Mater.*, 2008, **154**, 44-50.
19. M.S. Miao, Y.J. Zhang, L. Shu, J. Zhang, Q. Kong and N. Li, *Int. Biodeterior. Biodegrad.*, 2014, **95**, 61-66.
20. A. G. Jesus, F. J. Romano-Baez, L. Leyva-Amezcua, C. Juarez-Ramirez, N. Ruiz-Ordaz and J. Galindez-Mayer, *J. Hazard. Mater.*, 2009, **161**, 1140-1149.
21. K. H. Kung and M. B. McBride, *Environ. Toxicol. Chem.*, 1991, **10**.
22. M. B. McBride and K. H. Kung, *Environ. Sci. Technol.*, 1991, **25**, 702-709.
23. B. Okolo, C. Park and M. A. Keane, *J. Colloid Interface Sci.*, 2000, **226**, 308-317.
24. M. Ó. C. Michael J. Hynes, *J. Inorg. Biochem.*, 2001, **85**, 131–142.
25. K. F. Pirker, M. C. Baratto, R. Basosi and B. A. Goodman, *J. Inorg. Biochem.*, 2012, **112**, 10-16.
26. M. J. Hynes and Mairtın Ó'Coinceanainn, *J. Inorg. Biochem.*, 2001, **84**, 1-12.
27. X. Zhang, Y. Hou, P. Hu and C. Hong, *J. Eur. Ceram. Soc*., 2012, **32**, 3463-3468.
28. S. Tascioglu, O. Sendil and S. Beyreli, *Anal. Chim. Acta*, 2007, **590**, 217-223.
29. B. I. Ipe, S. Cherumuttathu, H. Y. Karuvath, Thomas K. George, *J. Phys. Chem.*, 2007, **111**, 12839-12847.
30. D. Feng, T. F. Liu, J. Su, M. Bosch, Z. Wei, W. Wan, D. Yuan, Y. P. Chen, X. Wang, K. Wang, X. Lian, Z. Y. Gu, J. Park, X. Zou and H. C. Zhou, *Nat. commun.*, 2015, **6**, 5979.
31. S. Chavan, J. G. Vitillo, D. Gianolio, O. Zavorotynska, B. Civalleri, S. Jakobsen, M. H. Nilsen, L. Valenzano, C. Lamberti, K. P. Lillerud and S. Bordiga, *Phys. Chem. Chem. Phys*, 2012, **14**, 1614-1626.
32. H. R. Abid, H. M. Ang and S. Wang, *Nanoscale*, 2012, **4**, 3089-3094.
33. J. David, G. Trolliard, C. Volkringer, T. Loiseau and A. Maître, *Phys. Rev. Lett.*, 2015, **5**, 51650-51661.

34. A. M. Ebrahim and T. J. Bandosz, *ACS Appl. Mater Interfaces*, 2013, **5**, 10565-10573.
35. F. Heshmatpour and R. B. Aghakhanpour, *Adv. Powder Technol.*, 2012, **23**, 80-87.
36. A. K. Singh, *Adv. Powder Technol.*, 2010, **21**, 609-613.
37. J. B. DeCoste, G. W. Peterson, H. Jasuja, T. G. Glover, Y. G. Huang and K. S. Walton, *J. Mater. Chem.*, 2013, **1**, 5642.
38. J. Long, S. Wang, Z. Ding, S. Wang, Y. Zhou, L. Huang and X. Wang, *Chem. Commun.*, 2012, **48**, 11656-11658.
39. J. Wang, T. Shi and X. Jiang, *Nanoscale Res. Lett.*, 2008, **4**, 240-246.
40. I. Langmuir, *J. Am. Chem. Soc.*, 1918, **40**, 1361-1403.
41. Y. Tanaka, M. Nakai, T. Akahori, M. Niinomi, Y. Tsutsumi, H. Doi and T. Hanawa, *Corros. Sci.*, 2008, **50**, 2111-2116.
42. I. Sabbah and M. Rebhun, *Water Environ. Res.*, 1997, **69**, 1032-1038.
43. C. Karunakaran, R. Dhanalakshmi and P. Gomathisankar, *Spectrochim. Acta, Part A*, 2012, **92**, 201-206.

Table 1 The pseudo-first-order and pseudo-second rate constants for the adsorption of TCP on ZrO_2-C

	$q_{e,exp}$ (mg g^{-1})	Pseudo-first-order			Pseudo-second-order		
		$q_{e,cal}$ (mg g^{-1})	k_1 (h^{-1})	R^2	$q_{e,cal}$ (mg g^{-1})	K_2 (h^{-1})	R^2
TCP	306	158	0.2524	0.9146	312.5	0.0039	0.9974

489 **Table.2** Langmuir and Freundich parameters for the adsorption of TCP on ZrO_2-C at

490 different temperature

Solution temperature(K)	Langmuir isotherm model			Freundlich isotherm model		
	Q_0 (mg g^{-1})	K_L (L mg^{-1})	R^2	K (mg g^{-1}(L mg^{-1})$^{1/n}$)	1/n	R^2
303	454.5	0.090	0.7489	32.422	0.749	0.9863
313	476.2	0.095	0.8139	34.655	0.743	0.9906
323	476.2	0.117	0.9401	38.303	0.748	0.9941

491

492

493 **Table 3** summarizes the comparison of TCP adsorption capacity on various

494 adsorbents

Adsorbent	T(K)	Q_e (mg g^{-1}) (C_0=20 mg L^{-1})	Reference
Zirconium dioxide-carbon	303	306	This study
Graphene oxide	303	190	[6]
Coconut husk-based activated carbon	303	122	[5]
Graphene	298	50	[7]
CFAC	293	192	[9]
Coconut shell-based activated carbon	303	112	[4]
MMC	303	210	[10]
Commercial activated carbon	303	20	[4]
Activated clay	303	123	[12]

495

496 **Table 4** Thermodynamic parameters calculated

ΔH^0 (KJ mol^{-1})	ΔS^0 (J mol^{-1} K^{-1})	ΔG^0 (KJ mol^{-1} K^{-1})		
		303K	313K	323K
4.105	38.49	-7.56	-7.94	-8.33

497

498

Figures Captions

Fig.1. SEM images of Zr-GA (A) and ZrO_2-C (D), TEM images of Zr-GA(B, C), Zr-GA-C(E, F) , HRTEM image of ZrO_2-C(G).

Fig.2. XRD spectra of GA, Zr-GA and ZrO_2-C from 2**θ**=5 to 80˚

Fig.3. FTIR spectra of GA, Zr-GA and ZrO_2-C (A) and FTIR spectra of GA and Zr-GA in the region of 400-1800 cm^{-1} (B).

Fig.4. The fitted XPS O1s spectra (A) and Zr3d core level lines (B) of Zr-GA and ZrO_2-C, Raman spectra (C), TGA curves (D) and N_2 adsorption/desorption isotherm (E) of ZrO_2-C. Inset D describes the calculated pore size distribution of ZrO_2-C.

Fig.5. Effect of time (A) and solution pH (B) and ionic strength (D) on TCP adsorption to ZrO_2-C; ζ-potential of ZrO_2-C at different solution pHs (C).

Fig. 1

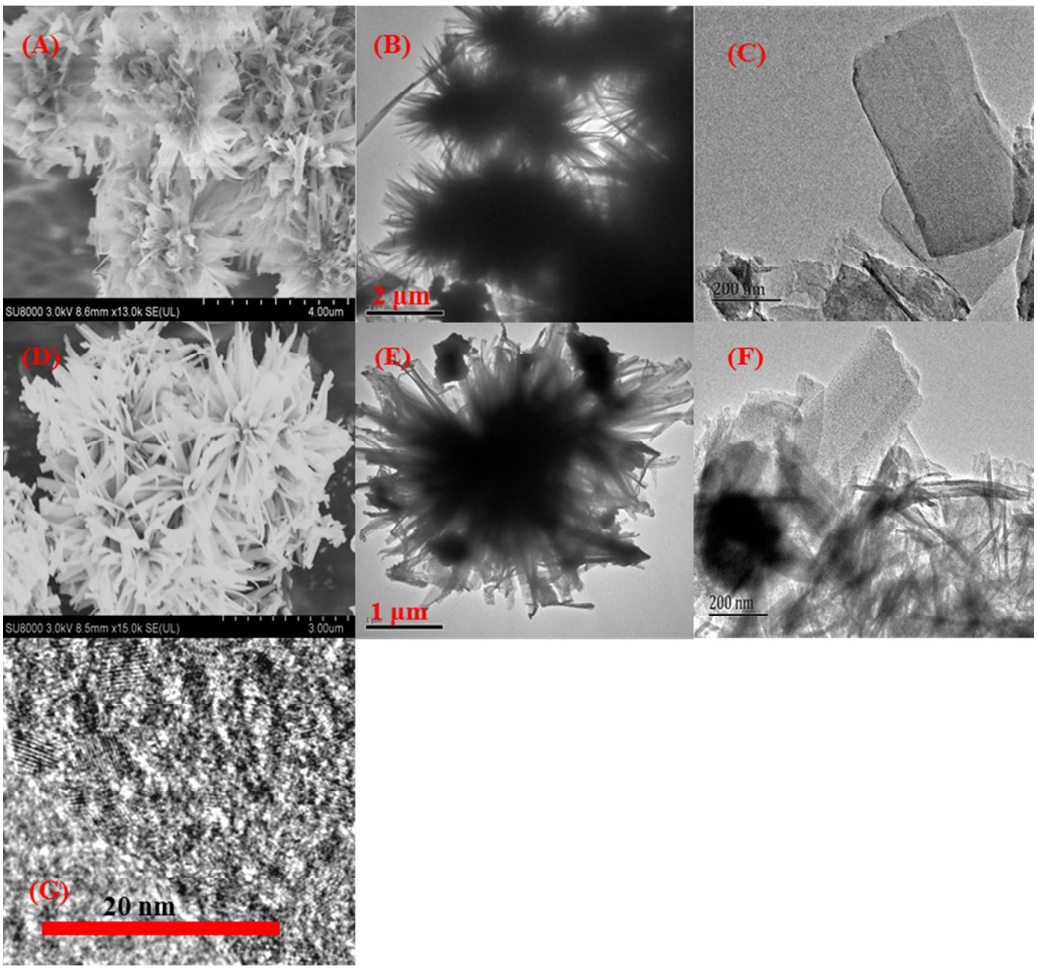

Fig. 2

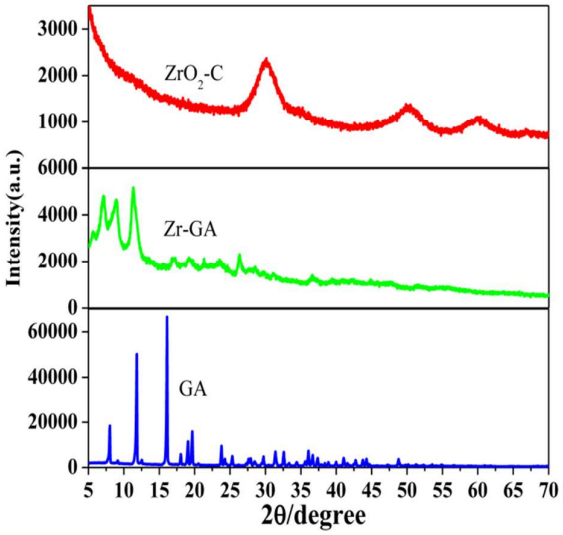

Fig. 3

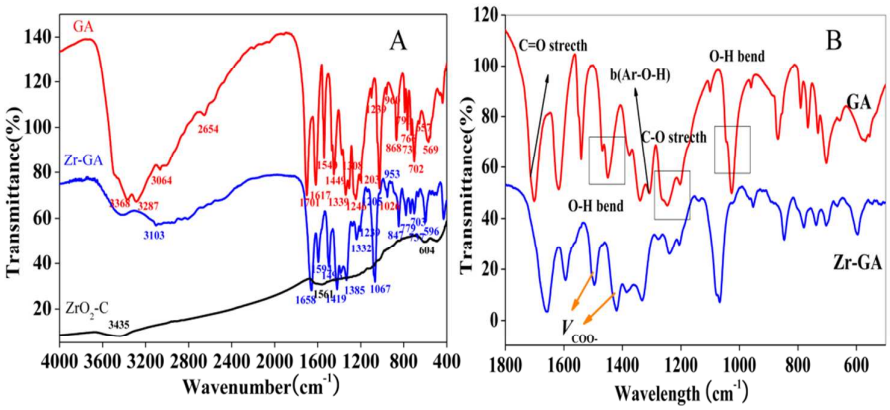

Fig. 4

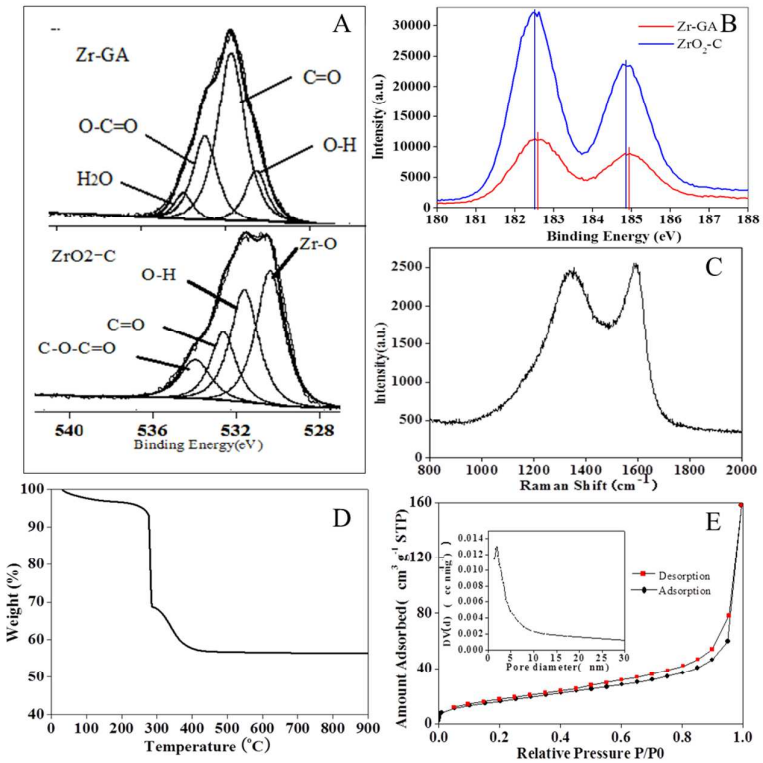

610 **Fig. 5**

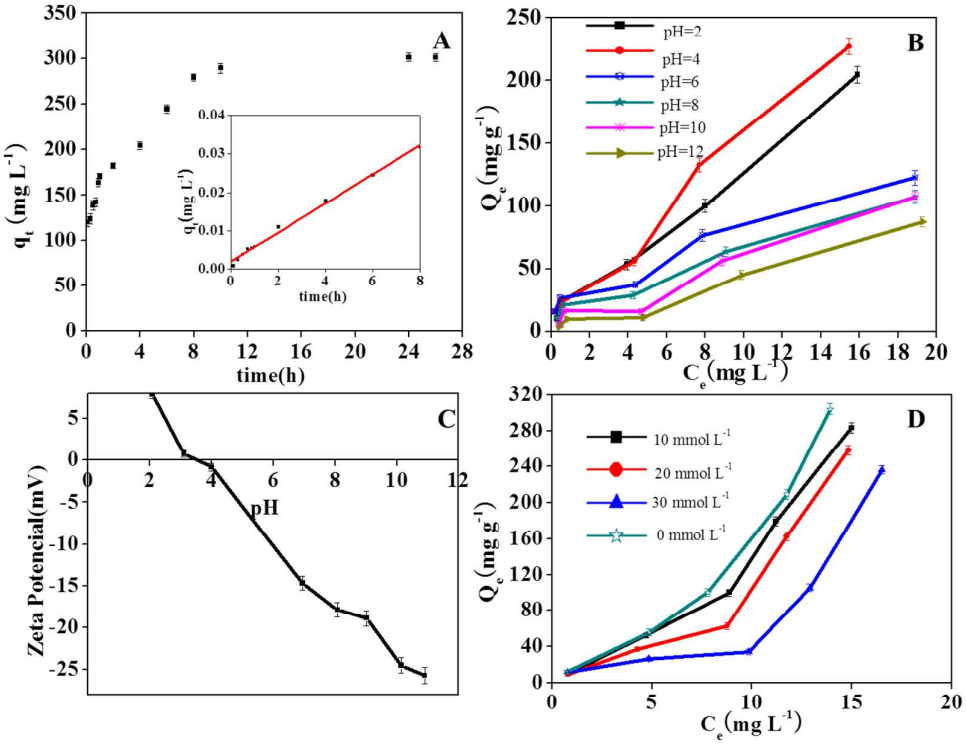

611